scientific reports

Check for updates

OPEN

Preparation and performance control of ultra-low near-infrared reflectivity coatings with super-hydrophobic and outstanding mechanical properties

Weigang Zhang[1]✉, Yueting Zhuang[1,2], Jialun Zhang[1,2] & Qianfeng Zhang[2]

The development of ultra-low near-infrared reflectivity coatings with outstanding engineering properties remains a challenge in laser stealth materials research. Herein, we reported a laser stealth coating with outstanding mechanical properties, super-hydrophobicity, and an ultra-low near-infrared reflectivity for 1.06 μm wavelength. The effects of the mass ratio of graphene to nano-SiO_2, the proportion of total filler, the addition of KH560, the mass ratio of Polydimethylsiloxane (PDMS) to acrylic-modified polyurethane (APU), and the addition of dioctyl phthalate (DOP) on the coating properties were thoroughly discussed. The coating can achieve a low reflectivity of 9.3% at 1.06 μm and a high water contact angle of 152° at a mass ratio of 7:3 for PDMS to APU and 6:4 for graphene to nano-SiO_2 with a total filler amount of 40 wt%. KH560 can play a bridging role between the blended resin matrix and nano-SiO_2, which can significantly improve the impact strength of the coating. The DOP, which contains a polar ester group and a non-polar carbon chain structure, can be inserted between the molecular chains of the resin to weaken the intermolecular force of the resin, so that the flexibility of the coating can be significantly improved. Adding KH560 at 4 wt% and DOP at 1 wt%, resulted in a coating with ultra-low near-infrared reflectivity of 1.06 μm (9.3%), super-hydrophobic properties, outstanding adhesion strength (grade 2), flexibility (2 mm), and impact strength (50 kg cm). The above super-hydrophobic ultra-low near-infrared reflectivity coating has significant potential for use in the field of laser stealth equipment, and it can serve as a useful reference for optimizing the mechanical properties of super-hydrophobic functional coatings.

Keywords Super-hydrophobic, Ultra-low near-infrared reflectivity, Composite coating, Mechanical property optimization

With the rapid advancement of modern military technology, the requirement of stealth coating on all kinds of equipment is increasing. Because the coating surface is exposed to the complex battlefield environment rich in dust and other pollutants for an extended period of time, the coating's stealth performance, adhesion strength, flexibility, impact strength, and appearance are damaged. In particular, the gradual loss of stealth effect may result in serious battlefield security issues for weapons and equipment[1,2]. According to the 'lotus effect', the hydrophobicity of the coating can be improved[3,4], which can spontaneously clean the surface pollutants to effectively improve the service life of the stealth coating. Therefore, when designing stealth coatings, it is necessary to consider the effective compatibility of the stealth effect and super-hydrophobic properties.

Super-hydrophobic functional materials with a WCA greater than 150° have excellent waterproof, anti-fouling, anti-corrosion, and self-cleaning properties, and have a wide range of applications[5–8]. The resistance

[1]College of Materials and Chemical Engineering, Chuzhou University, Hui Feng Road 1, Chuzhou 239000, China. [2]Engineering Research Institute, Anhui University of Technology, Hudong Road 59, Maanshan 243000, China. ✉email: abczwg15@163.com

of solids to wetting is primarily determined by the interplay between the surface roughness structure and the presence of low surface energy materials[9–11]. Research has demonstrated that creating micro-nano rough structures on the surface of low-surface energy materials can enhance air contact and promote the formation of additional gas–liquid interfaces. This leads to a notable increase in the contact angle between the liquid and solid surfaces[12,13]. However, materials with high roughness and low surface energy often have poor binding with the substrate, making it difficult to meet the mechanical properties requirements of super-hydrophobic materials in practical applications. To resolve this issue, numerous efforts have been made to transform hydrophilic materials into super-hydrophobic materials. Meng et al. used air injection to combine the uncured PDMS adhesive with SiO_2 to prepare a hydrophobic coating that can be successfully applied on the circuit board[14]. Zhang et al. synthesized an aqueous super-hydrophobic coating with a concentration of 42% in a mixed solvent of ethanol and water using an appropriate amount of nano-SiO_2 and PVP protective polymer as the main raw materials[15]. C. Anitha added metal silicate, nano-SiO_2, nano-TiO_2, and aluminum stearate into silicone resin to prepare a super-hydrophobic coating with outstanding performance using the spraying method[16]. In addition, due to its unique micro-structure, graphene has distinctive photoelectromagnetic properties, which have important applications in the field of water zinc-ion batteries and electromagnetic interference shielding[17,18].

The above materials have made remarkable progress in single super-hydrophobic performance and the functional characteristics of various stealth materials. Han et al. prepared samarium oxysulfide using the flux method, which has a low reflectivity at 1064 nm[19]. Chai et al.[20] prepared a multi-band compatible stealth material by modifying Cr_2O_3 with silver and colored pigments with low emissivity materials. In the early stage of their research, a multi-spectrum compatible coating with an infrared emissivity of 0.506 and 1.06 μm near-infrared reflectivity of 41.6% was prepared using the glass rod scraping method[21]. In addition, this research group has also developed earth yellow and medium green ultra-low near-infrared reflectivity coatings[22]. The effective stealth capabilities of the material rely not just on the functional properties of the filler, but also on the presence of polar bonds between the resin matrix and the filler. These bonds create a robust interface bond and enhance the material's micro-structure, facilitating the enhancement of its functional properties[23,24]. Improving the micro-interface structure and surface energy of materials is the primary focus and challenge of this project. Overcoming this issue is of great significance for achieving good super-hydrophobic and mechanical properties of stealth materials.

In this study, the glass rod scraping coating method was used to prepare composite coatings with APU as an adhesive, PDMS as a blend modifier, graphene as a near-infrared absorber, and nano-SiO_2 as a modified filler for rough surface structure. Graphene was introduced into the coating to achieve ultra-low near-infrared reflectance, nano-SiO_2 to achieve super-hydrophobic performance, and interface modifiers such as KH560 and DOP to optimize the coating's overall performance. The reflectivity at the wavelength of 1.06 μm and the WCA of the coatings were systematically studied. The effects of the amount of graphene, nano-SiO_2, APU, PDMS, KH560, and DOP on the micro-structure, mechanical properties, WCA, and 1.06 μm near-infrared reflectivity of the coatings are discussed in detail. The prepared super-hydrophobic and ultra-low near-infrared reflectivity coatings have a wide range of potential applications in various laser stealth equipment.

Experiment

Materials

Multilayer graphene (Gr, purity 95 wt%, thickness 3–8 nm, particle size 5–50 μm, number of layers 5–10, specific surface area 2600–3000 m^2/g), Nano-SiO_2 (purity 99.99 wt%, diameter 10–30 nm, specific surface area 100–500 m^2/g), Acrylic modified polyurethane (APU, liquid, solid content 66.67 wt%), APU curing agent (liquid, solid content 33.24 wt%), polydimethylsiloxane (PDMS, liquid, solid content 99.99 wt%), PDMS curing agent (liquid, solid content 99.99 wt%), KH560 (liquid, purity 99.99 wt%), DOP (dioctyl phthalate, a commonly used plasticizer, liquid, purity 99.99 wt%), the diluent is composed of butyl acetate and acetone by mass ratio of 1:1, tinplate substrate (12 cm × 5 cm × 0.28 mm). All other reagents are analytically pure. APU and supporting curing agent are mixed with a 2:1 mass ratio as coating binder, while PDMS and supporting curing agent are mixed in a 10:1 mass ratio as modified resin.

Coating preparation

After polishing the tinplate substrate with 360-mesh sandpaper, wipe the surface of the substrate with anhydrous ethanol, and put it aside for half an hour. The modified resin was obtained by the blending modification method. APU and PDMS with a mass ratio of 4:6 were first weighed in a clean disposable plastic cup and thoroughly stirred with a glass rod to obtain the blended APU with PDMS. Then, the total filler was set to 30 wt%, with varying mass ratios (4:6, 5:5, 6:4, 7:3, and 8:2) of graphene to nano-SiO_2 composite filler mixed with the above-modified resin, and an appropriate amount of diluent was added to adjust viscosity. The mixture was then subjected to an ultrasonic wave of 50 W for 5 min to ensure that the resin matrix and the functional filler were thoroughly mixed, resulting in the fine dispersion of the paint. No obvious particles could be seen in the paint, and the paint had good fluidity. A certain amount of APU curing agent and PDMS curing agent was added according to the fixed ratio, and the paint product was obtained after evenly mixing. Subsequently, the paint was uniformly applied to the tinplate surface using the glass rod scraping coating method. The coating was allowed to dry at room temperature for 6 h before baking in an oven at 120 °C for 3 h to produce the coating sample for testing. The appropriate mass ratio of graphene and nano-SiO_2 was determined based on the near-infrared reflectivity, WCA, and mechanical properties of the coating. Using the same coating preparation method, based on the best mass ratio of graphene to nano-SiO_2, the effects of total filler additions (10 wt%, 20 wt%, 30 wt%, 40 wt%, and 50 wt%), KH560 content (0 wt%, 2 wt%, 4 wt%, 6 wt%, and 8 wt%), the mass ratio of APU to PDMS (1:9, 2:8, 3:7, 4:6, and 5:5), and DOP content (0 wt%, 1 wt%, 3 wt%, 5 wt%, and 7 wt%) on the properties of the coating were studied. Finally, a super-hydrophobic ultra-low near-infrared reflectivity coating with good

flexibility, excellent adhesion strength, and impact strength was obtained. The coating preparation process is shown in Fig. 1.

Characterization

The microstructure, near-infrared reflectance spectrum, WCA, adhesion strength, flexibility, and impact strength of the coating were studied in this paper. The micro-structure was characterized by scanning electron microscopy (JSM-6510LV, Japan Electronics Corporation, Tokyo, Japan). The near-infrared reflectance spectrum was measured by a UV–VIS-NIR spectrophotometer (UV-3600, Shimadzu Corporation of Japan, Tokyo, Japan). The WCA was measured by a CA measuring instrument (JC2000D7, Shanghai Zhongchen Co., Ltd, Shanghai, China). The adhesion strength of the coating was evaluated by a QFZII adhesion tester (GB 1720-79). The flexibility of the coating was evaluated by a QTY-10A cylindrical bending tester (GB/T 1731-93). The impact strength of the coating was tested by a QCJ impact strength tester (GB/T 1732-93).

Results and discussion

Effect of m_{Gr}:$m_{nano\text{-}SiO_2}$ on coating properties

The SEM images of the coatings prepared by m_{Gr}:$m_{nano\text{-}SiO2}$ at 4:6, 6:4, and 8:2 are shown in Fig. 2 when mAPU:mPDMS is 4:6 and the total filler amount is 30 wt%. The surface micro-structure of the coating varies significantly depending on the mass ratios of graphene to nano-SiO_2. When the mass ratio of graphene to

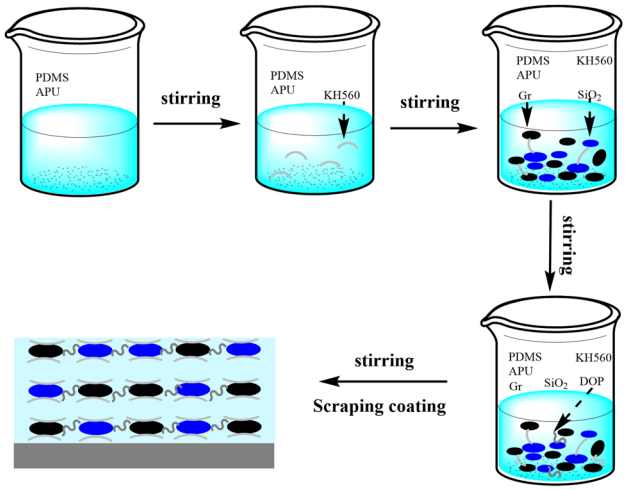

Fig. 1. Flow chart of coating preparation.

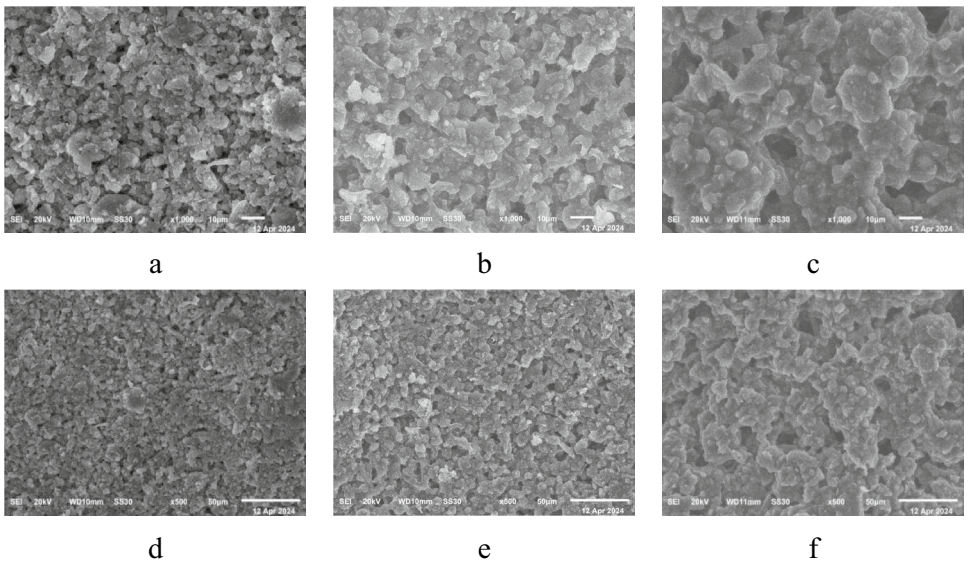

Fig. 2. SEM images of coatings with varying m_{Gr}:$m_{nano\text{-}SiO2}$, (**a**, **d**) 4:6, (**b**, **e**) 6:4, and (**c**, **f**) 8:2.

nano-SiO_2 increases, the surface particle characteristics formed by nano-SiO_2 agglomeration significantly weaken, the lamellar structure characteristics of multilayer graphene enhance, and the coating surface becomes more compact. When m_{Gr}:$m_{nano\text{-}SiO2}$ is 4:6, the flake graphene is evenly divided into the resin and nano-SiO_2, and a large amount of nano-SiO_2 is distributed on the surface of the coating, leading to a rough surface texture with a surface roughness of 2–6 μm. When m_{Gr}:$m_{nano\text{-}SiO2}$ is 6:4, its dispersion in the resin matrix is more uniform due to the large specific surface area of graphene and its good compatibility with APU-modified PDMS[25,26]. This reduces the surface roughness of the coating and increases its regularity. When m_{Gr}:$m_{nano\text{-}SiO2}$ is 8:2, the graphene content is more, the nano-SiO_2 content is less, and the graphene is fully dispersed in the resin, the coating surface structure is dense, and the rough structure is almost eliminated.

Figure 3 shows the WCAs of the coatings with varying m_{Gr}:$m_{nano\text{-}SiO2}$ of 4:6, 6:4, and 8:2. It can be seen that as the mass ratio of graphene to nano-SiO_2 increases the micro-nano rough structure and the WCA decreases. When m_{Gr}:$m_{nano\text{-}SiO2}$ is 4:6, the WCA reaches 149.5°, owing to the extensive distribution of nano-SiO_2 on the coating surface. There are more mastoid-shaped micro-nano rough structural units constructed by resin matrix and nano-SiO_2 on the surface. A large number of mastoid-shaped micro-nano rough structures will increase the contact between the liquid phase and gas phase, thereby increasing the WCA between solid and liquid[27]. When m_{Gr}:$m_{nano\text{-}SiO2}$ is 6:4, the roughness of the coating surface is reduced, and the high specific surface area of graphene increases the surface energy of the coating, thus reducing the WCA.

Figure 4 displays the near-infrared reflectance spectra of the coatings at various mass ratios of graphene to nano-SiO_2. The near-infrared reflectivity of coatings with the same total filler addition amount is lower than 10% in the tested near-infrared range. Moreover, the reflectivity of the coating gradually decreases with the increase of m_{Gr}:$m_{nano\text{-}SiO2}$. The near-infrared reflectance at 1.06 μm decreases from 8.4% at m_{Gr}:$m_{nano\text{-}SiO2}$ = 4:6 to 6.4% at m_{Gr}:$m_{nano\text{-}SiO2}$ = 8:2. The reduction of nano-SiO_2 content causes the coating surface to become more regular. In addition, the graphene microstructure is composed of a large number of benzene ring structures, and it has an extremely long and complex conjugated system. Therefore, it strongly absorbs near-infrared light, and its incorporation into the coating can achieve ultra-low near-infrared reflectivity. Additionally, as the graphene content increases, it becomes fully dispersed in the resin matrix, resulting in better coverage of the nano-SiO_2 particles. This enables the coating to efficiently absorb near-infrared light and reduce near-infrared reflectivity.

Table 1 displays the adhesion strength, flexibility, and impact strength of the coatings at various m_{Gr}:$m_{nano\text{-}SiO2}$ ratios. The adhesion strength, flexibility, and impact strength of the coating are affected by varying mass ratios of graphene and nano-SiO_2. Overall, the mechanical characteristics of the coating improved as the m_{Gr}:$m_{nano\text{-}SiO2}$

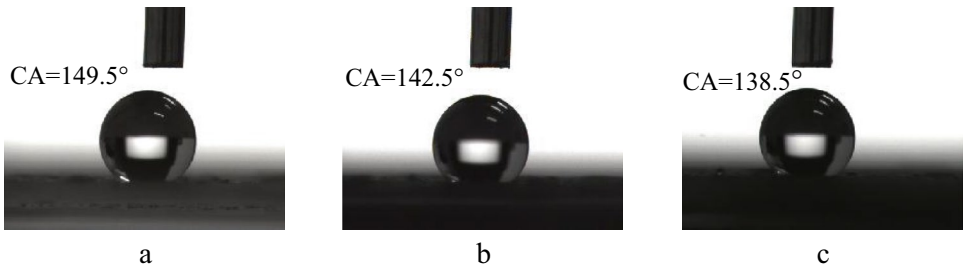

Fig. 3. WCAs of coatings with varying m_{Gr}:$m_{nano\text{-}SiO2}$, (**a**) 4:6, (**b**) 6:4, and (**c**) 8:2.

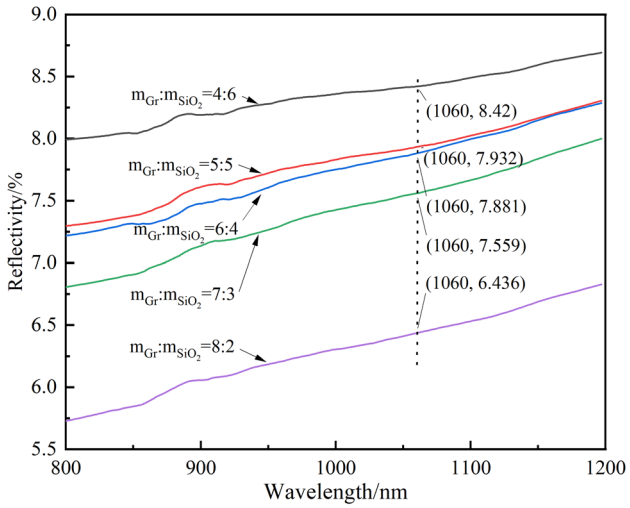

Fig. 4. Near-infrared reflectance spectra of the coatings with varying m_{Gr}:$m_{nano\text{-}SiO2}$ ratios.

m_{Gr}:$m_{nano\text{-}SiO2}$	4:6	5:5	6:4	7:3	8:2
Adhesion strength/grade	4	1	1	1	1
Flexibility/mm	8	6	5	4	3
Impact strength/kg × cm	10	10	15	15	40

Table 1. Mechanical properties of coatings with varying m_{Gr}:$m_{nano\text{-}SiO2}$.

ratio increased. When m_{Gr}:$m_{nano\text{-}SiO2}$ = 4:6, the coating demonstrated poor adhesion strength, flexibility, and impact resistance. The reason for this phenomenon is that when the nano-SiO_2 content is high in the coating, the resin matrix cannot completely cover the filler particles, resulting in ineffective formation of the coating. Furthermore, the coating contains a significant amount of micro-pores, leading to the presence of a weaker boundary layer within the coating, ultimately resulting in poor mechanical properties[28,29]. As m_{Gr}:$m_{nano\text{-}SiO2}$ increases, the special planar network structure, the coordination relationship between carbon atoms, and the special chemical bonding properties of graphene enhance the chemical bonding energy between the resin matrix and the filler. Consequently, greater force is required to damage the coating structure. As a result, the coating's mechanical properties are gradually enhanced[30,31]. Considering the near-infrared absorption properties, hydrophobic properties, and mechanical properties of the coating, the optimum mass ratio of graphene to nano-SiO_2 in the coating is determined to be 6:4.

Effect of total filler addition amount on coating performance

Figure 5 shows SEM images of the coatings prepared under the curing temperature of 120 °C, APU to PDMS mass ratio of 4:6, graphene to nano-SiO_2 mass ratio of 6:4, and total filler amount of 10 wt%, 30 wt%, 40 wt%, and 50 wt%. It shows that the roughness of the coating surface increases with total filler content. At the total filler amount of 50 wt%, the surface roughness of the coating can reach 3–8 μm. In addition, the surface porosity of the coating increases while its density decreases. When the filler content in the coating is 10 wt%, the composite fillers composed of graphene and nano-SiO_2 are scattered throughout the coating and cannot cover the entire coating, there are more resins between the functional fillers, and the surface is very smooth. As the composite filler content increased to 30 wt%, the density of graphene and nano-SiO_2 distributed in the coating increased significantly, but the coating still had a large and thick resin matrix. When the total filler content reaches 40 wt%, a significant number of micro-nano rough structural units composed of nano-SiO_2 and resin matrix develop on the coating surface. These rough structural units enhance the coating's wetting resistance, leading to improved hydrophobic performance. In addition, as the amount of composite fillers in the coating increases, the content of graphene also increases and becomes more evenly dispersed in the resin and nano-SiO_2. This increased dispersion improves the coating's ability to absorb incident near-infrared light, resulting in relatively low reflectivity at 1.06 μm, thereby meeting the requirements of laser stealth. When the coating contains an excessive amount of composite fillers (Fig. 5d, h), the nano-SiO_2 particles push out each other, increasing the surface roughness of the coating and causing a large number of pores to appear, significantly weakening the mechanical properties of the coating.

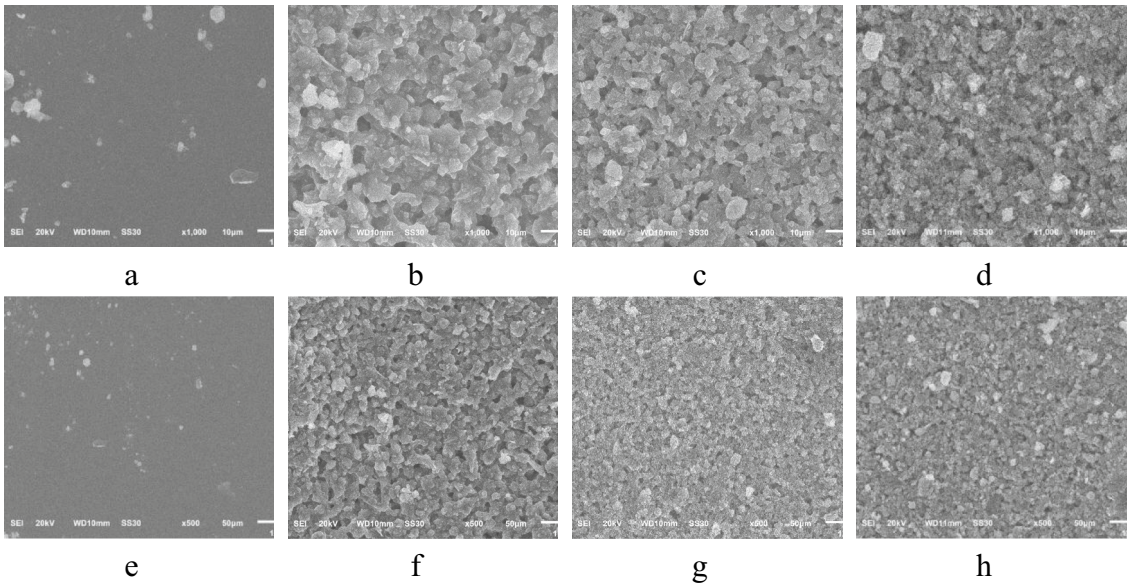

Fig. 5. SEM images of coatings with varying total filler additions, (**a**, **e**) 10 wt%, (**b**, **f**) 30 wt%, (**c**, **g**) 40 wt%, and (**d**, **h**) 50 wt%

Figure 6 displays the WCAs of the coatings with varying total filler additions. It shows that the WCA of the coating increases significantly with the increase in the total filler content. When the total fill content is 10 wt%, the WCA is only 98.5°, indicating a poor hydrophobic effect. This is because the surface of the coating is mainly a resin matrix and relatively thick, preventing the hydrophobic nano-SiO_2 from spreading on the surface of the coating, resulting in a low hydrophobicity of the coating. With the increase of the total filler content, the roughness of the coating surface also increases, and the micro-nano rough structural units with mastoid structure characteristics increase significantly, resulting in lower surface energy and larger WCA. When the total filler content is 50 wt%, the coating has a WCA of 152.5°, indicating super-hydrophobic properties.

Figure 7 shows the near-infrared reflectance spectra of the coatings with varying total filler additions. The reflectivity of the coating at 1.06 μm decreases from 7.7% with a total filler addition of 10 wt% to 4.2% with a total filler addition of 20 wt% and then increases to 13.6% with a total filler addition of 50 wt%. The reason for this phenomenon is that graphene has excellent near-infrared absorption properties[21,22]. Even with a total filler proportion of only 10 wt%, a small amount of uniformly dispersed graphene in the coating can still efficiently absorb near-infrared light. This reduces the coating's reflectivity at 1.06 μm to as low as 7.7%. When the proportion of total filler increased to 20 wt%, the absolute content of graphene in the coating also increased and remained evenly dispersed. This enhanced the coating's absorption of near-infrared light and reduced reflectivity to as low as 4.2% at 1.06 μm. However, as the total filler content increased, the reflectivity of the coating to near-infrared light increased. The primary factor is that as the total filler amount in the coating continues to rise, so does the absolute content of nano-SiO_2, which not only has no absorption effect on near-infrared light, but also has a certain reflection effect. In addition, when the proportion of total filler is too large, it will not only increase the gap on the surface of the coating, but also easily cause a large number of nano-SiO_2 to gather on the surface of the coating and weaken the absorption of the coating to near-infrared light. When the total filler content is too high, the near-infrared light absorption of the coating is reduced due to the combined action of the above factors.

Table 2 shows the adhesion strength, flexibility, and impact strength of the coatings under different proportions of total fillers. It shows that the adhesion strength is reduced from grade 1 with a total filler volume of 10 wt% to grade 2 with a total filler volume of 50 wt%, and the flexibility is reduced from 3 mm with a total filler volume of 10 wt% to 8 mm with a total filler volume of 50 wt%. The impact strength decreased from 40 kg × cm with a total packing volume of 10 wt% to 5 kg × cm with a total packing volume of 50 wt%. This phenomenon is primarily due to the fact that the polyurethane resin contains strong reactive polar groups, such as isocyanate groups, which can form a good interface bond with the filler. When the total filler is only 10 wt%, the content of

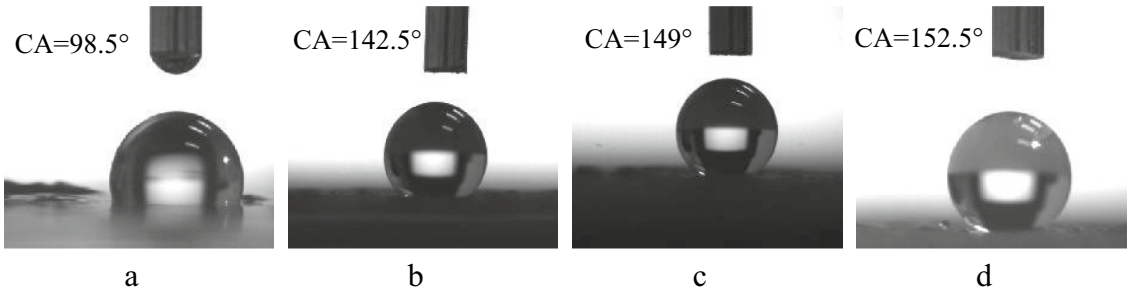

Fig. 6. WCAs of coatings with varying total filler additions, (**a**) 10 wt%, (**b**) 30 wt%, (**c**) 40 wt%, and (**d**) 50 wt%

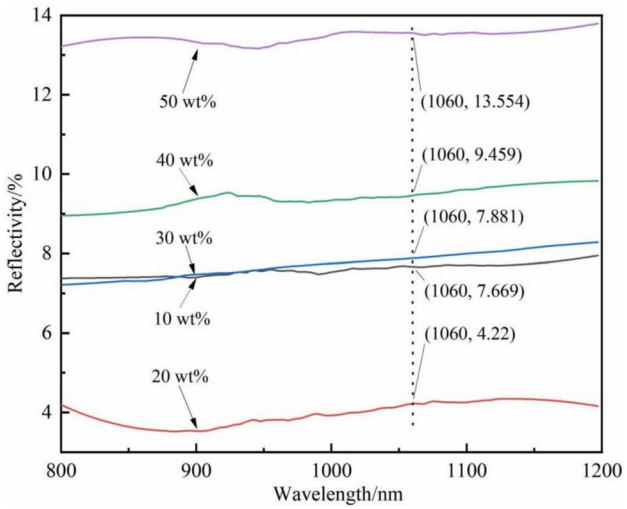

Fig. 7. Near-infrared reflectance spectra of the coatings with varying total filler additions.

Total filler addition/wt%	10	20	30	40	50
Adhesion strength/grade	1	1	1	2	2
Flexibility/mm	3	4	5	6	8
Impact strength/kg × cm	40	30	15	15	5

Table 2. Mechanical properties of coatings with varying total filler additions.

polyurethane resin is higher, and it has a strong binding force on the filler, resulting in the coating having excellent mechanical properties under these conditions. However, because the resin used in the coating contains PDMS with low surface energy, its binding to the filler is weak, resulting in suboptimal flexibility and impact strength of the coating when the total filler content is low. As the proportion of total filler increases, the content of resin decreases, as does the wrapping strength of resin on the filler and the corresponding binding force. Considering the near-infrared absorption, hydrophobic, and mechanical properties of the coating, the proportion of total fillers in the coating is determined to be 40 wt%.

Effect of KH560 on coating properties

Figure 8 shows SEM images of the coatings prepared under the following conditions: curing temperature of 120 °C, mass ratio of APU to PDMS of 4:6, mass ratio of graphene to nano-SiO_2 of 6:4, total filler addition of 40 wt%, and KH560 addition of resin mass of 0 wt%, 4 wt%, and 8 wt% According to the morphology of the coating surface, the addition of KH560 has little effect on the micro-structure of the coating. The resin in the coating is evenly mixed with graphene and nano-SiO_2 under different KH560 dosages, the resin layer thickness is suitable, and the graphene is evenly dispersed in the coating. Uniform and slightly agglomerated nano-SiO_2 particles can be seen on the surface of the coating, their arrangement is regular, and the structure is tight, leading to a clear micro-nano rough structure.

Figure 9 shows the WCAs of the coatings prepared with the addition of KH560 at 0 wt%, 4 wt%, and 8 wt% of the resin mass. It shows that the WCA can be increased from 149° without adding KH560 to 153° when adding 4 wt%, resulting in a coating with super-hydrophobic properties. As the amount of KH560 added to the coating increases, the influence of the coating's WCA is minimal. The reason is that the silico-oxygen bond in KH560 can

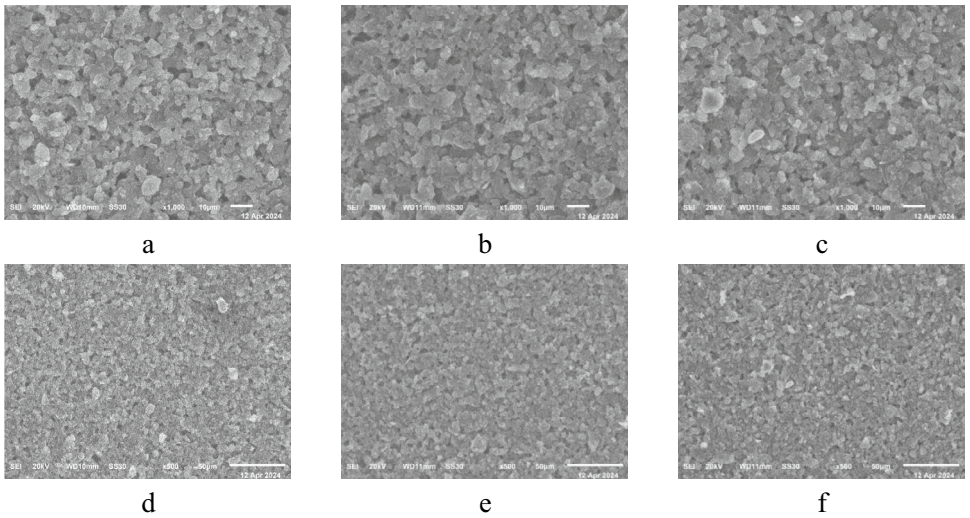

Fig. 8. SEM images of coatings with varying KH560 additions, (**a**, **d**) 0 wt%, (**b**, **e**) 4 wt%, and (**c**, **f**) 8 wt%

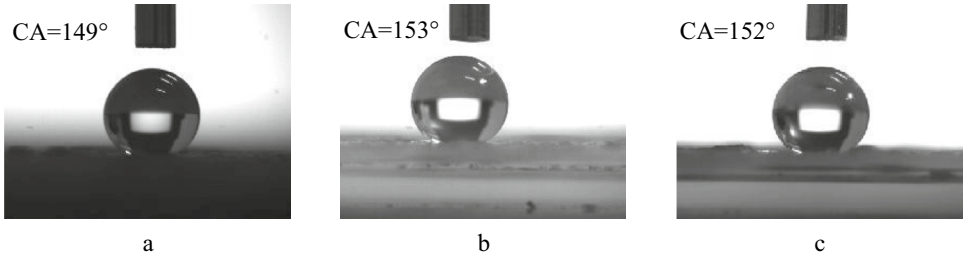

Fig. 9. WCAs of coatings with varying KH560 additions, (**a**) 0 wt%, (**b**) 4 wt%, and (**c**) 8 wt%

chemically react with the hydroxyl group on the surface of the inorganic material, forming a hydrophobic Si–O–Si group. This reaction lowers the surface energy of the coating, further enhancing its hydrophobic properties[32]. The specific action mechanism and process are shown in Fig. 10.

Figure 11 displays the near-infrared reflectance spectra of the coatings with varying KH560 additions. It can be seen that the modification of KH560 has little effect on the near-infrared reflectivity of the coating at 1.06 μm, with a variation of only 0.6%. The main reason is that when the ratio of fillers, the proportion of total fillers, and the ratio of resin remain constant, the addition of a small amount of KH560 has no significant effect on the micro-structure of the coating, and the graphene that absorbs near-infrared light is still evenly and widely distributed between the nano-SiO_2 and the resin. Even if the silicon-oxygen bond of KH560 interacts with PU, PDMS, and some inorganic fillers to increase the binding force between the adhesive and the filler, the resin thickness, the void between the filler and the resin, and the overall micro-structure of the coating change slightly. These minor changes have little effect on the near-infrared absorption capacity of the coating, allowing it to maintain outstanding near-infrared low reflectivity properties.

Table 3 shows the adhesion strength, flexibility, and impact strength of the coatings with different KH560 additions. The addition of KH560 did not affect adhesion strength and flexibility of the coating, but it significantly improved impact strength. Even a small amount of KH560 can increase the impact strength of the coating to its optimum level (50 kg × cm). This is attributed to the bridging effect of KH560 as a standard coupling agent. One end of the molecular structure of KH560 can react with groups such as silica bond and hydroxyl group in inorganic fillers to form covalent bonds, and the other end can engage with active groups like amino group,

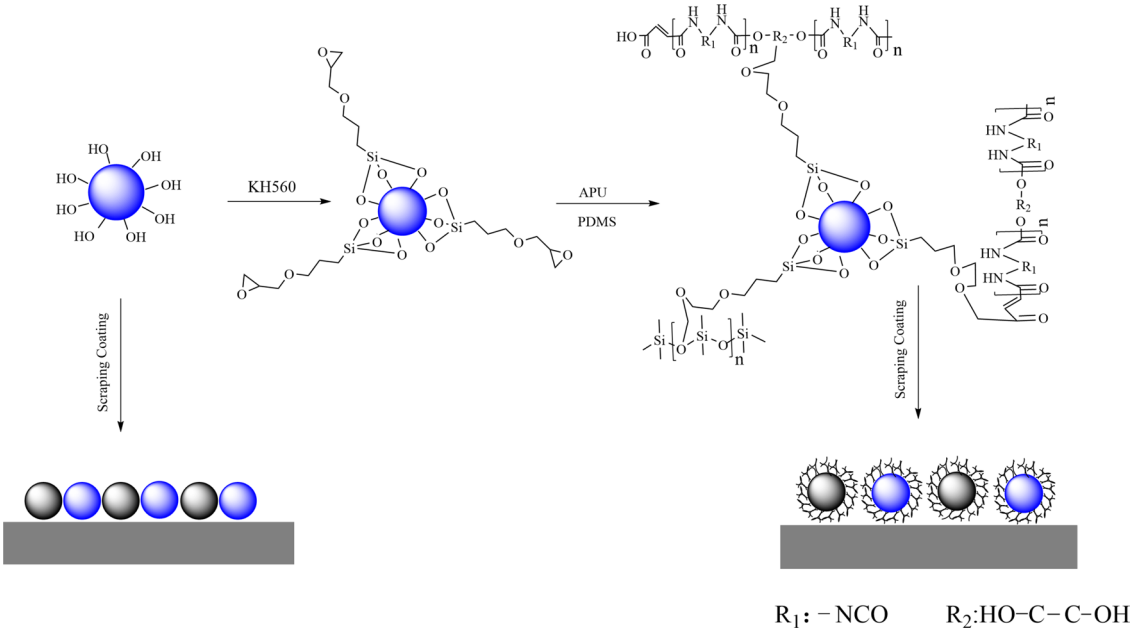

Fig. 10. Effect mechanism of KH560 on micro-structure of the coating.

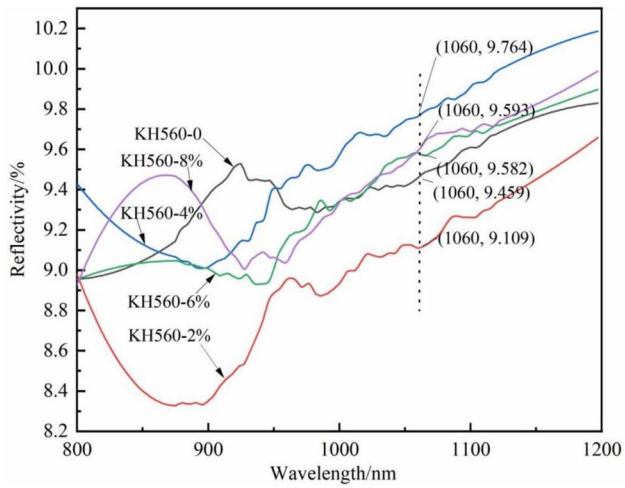

Fig. 11. Near-infrared reflectance spectra of coatings with varying KH560 additions.

Contents of KH560/wt%	0	2	4	6	8
Adhesion strength/grade	2	2	2	2	2
Flexibility/mm	6	6	6	6	6
Impact strength/kg × cm	15	50	50	50	50

Table 3. Mechanical properties of coatings with varying KH560 additions.

hydroxyl group, and carboxyl group present in the resin binder to establish chemical bonds. These interactions serve to improve the interface bonding strength between materials, and the adhesion strength between resin and substrate, resin and filler. The coating's impact strength is significantly enhanced in the end[33]. Considering the near-infrared absorption properties, hydrophobic properties, and mechanical properties of the coating, the optimal addition of KH560 in the coating is determined to be 4 wt%.

Effects of m_{APU}:m_{PDMS} on coating properties

Figure 12 shows SEM images of the coatings prepared under the following conditions: m_{Gr}:$m_{nano\text{-}SiO2}$ of 6:4, total filler addition of 40 wt%, KH560 addition of 4 wt%, and mass ratios of APU to PDMS of 1:9, 3:7, 4:6, and 5:5. As can be seen in Fig. 10a, a large mass ratio difference between APU and PDMS results in uneven local coating thickness, disordered and irregular distribution of nano-SiO_2, and a coating surface with large voids and high roughness. As m_{APU}:m_{PDMS} increases (Fig. 12b, c, d), the nano-SiO_2 in the coating becomes denser and more evenly distributed, and the graphene is also evenly dispersed, which makes the coating surface more regular and compact.

Figure 13 shows the WCAs of the coatings with varying m_{APU}:m_{PDMS} ratios of 1:9, 3:7, 4:6, and 5:5. As shown in the figure, the smaller the mass ratio of APU to PDMS, the larger the WCA of the coating. When the m_{APU}:m_{PDMS} ratio is 1:9, the coating exhibits a WCA of 158° and excellent super-hydrophobic properties. This occurs because

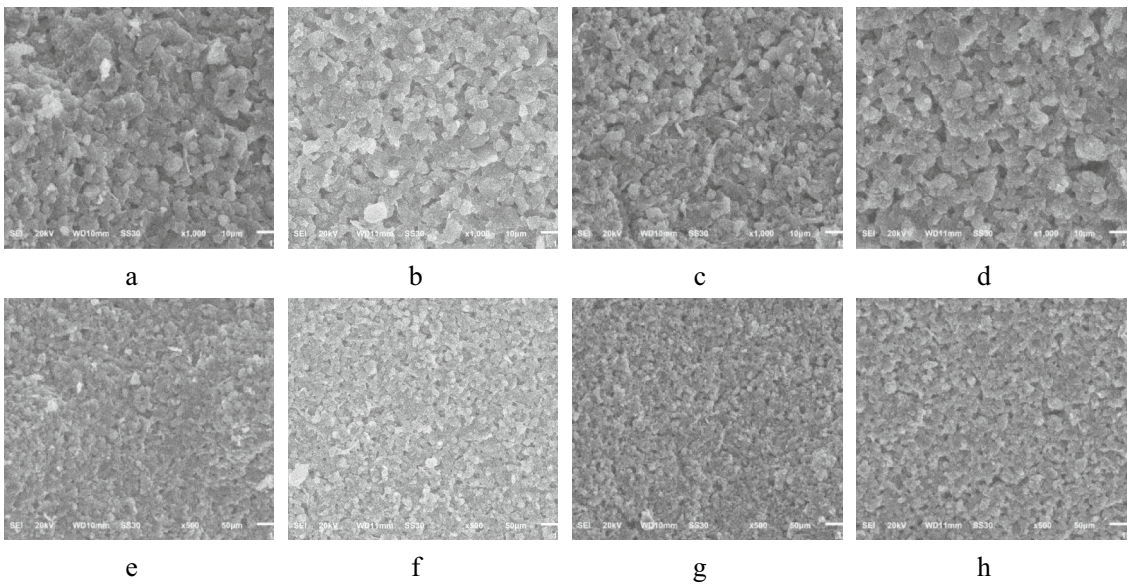

Fig. 12. SEM images of coatings with varying m_{APU}:m_{PDMS}, (**a**, **e**) 1:9, (**b**, **f**) 3:7, (**c**, **g**) 4:6, and (**d**, **h**) 5:5

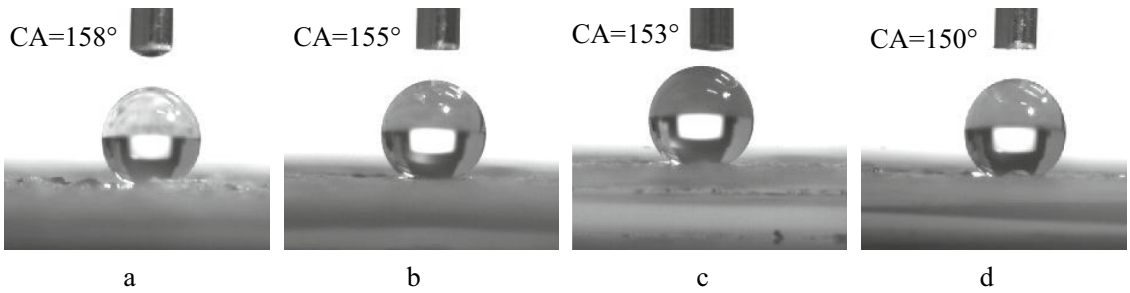

Fig. 13. WCAs of coatings with varying m_{APU}:m_{PDMS}, (**a**) 1:9, (**b**) 3:7, (**c**) 4:6, and (**d**) 5:5

PDMS, the main adhesive in the coating, consists mainly of a large number of non-polar silicon-oxygen-silicon bonds, which results in a very low surface energy. Consequently, the coating also has a very low surface energy, thereby optimizing its hydrophobic properties. As the mass ratio of APU to PDMS gradually increases, the absolute content of PDMS decreases, which reduces the organic content that can reduce the surface energy of the coating. Additionally, the APU utilized acrylic-modified polyurethane, which contains numerous robust polar groups such as hydroxyl and ether bonds that can establish hydrogen bonds with water molecules, enhancing the coating's wettability. As the mass ratio of APU to PDMS increases, so does the content of APU in the coating, and the wetting effect of the coating on water improves, reducing the WCA of the coating.

Figure 14 shows the near-infrared reflectance spectra of the coatings with varying m_{APU}:m_{PDMS} ratios. The coating has minimal effect on the reflectivity of 1.06 μm near-infrared light at various APU to PDMS mass ratios. The result shows that the adhesive has little effect on the laser stealth effect of the coating, and that graphene, as a near-infrared absorber, is the core factor that determines the ultra-low near-infrared reflectivity of the coating. Firstly, the stoichiometric numbers of graphene and nano-SiO_2 decreased with the increase of the mass ratio of APU to PDMS in the coating formulation, but the value change was only 0.04%, indicating that the change in graphene content had little effect on the composition of the whole formulation. Secondly, the change of m_{APU}:m_{PDMS} has very little effect on the micro-structure of the coating. Although the graphene content in the coating decreases slightly with the increase of m_{APU}:m_{PDMS}, its near-infrared reflectivity at 1.06 μm remains approximately 10%, maintaining outstanding laser stealth performance.

Table 4 shows the adhesion strength, flexibility, and impact strength of the coatings having different APU to PDMS mass ratios. It shows that the adhesion strength of the coating increases as the absolute content of PDMS decreases, while the flexibility deteriorates. However, the impact strength of the coating has been maintained in the best state due to the presence of KH560. When the absolute content of PDMS is high, the binding between resin, filler, and substrate is primarily determined by the silicon-oxygen bond in PDMS, which has high bond energy and very low binding force. As the absolute content of PDMS decreases, the absolute content of PU increases gradually, and the content of amino, hydroxyl, and carboxyl groups also increases. These groups readily establish covalent and hydrogen bonds with oxygen atoms or hydroxyl groups on the substrate's surface, consequently enhancing the adhesion strength of the coating. In addition, as the absolute content of APU increases, so do the strong reactive groups such as the isocyanate group and hydroxyl group, resulting in a significant increase in the cross-linking density. Consequently, the coating's hardness and brittleness increase, ultimately reducing flexibility. The impact strength of the coating is also always optimal thanks to the presence of KH560. To maintain near-infrared reflectivity at 1.06 μm below 10%, and achieve both super-hydrophobic and good mechanical properties, the optimal m_{APU}:m_{PDMS} ratio is determined to be 3:7.

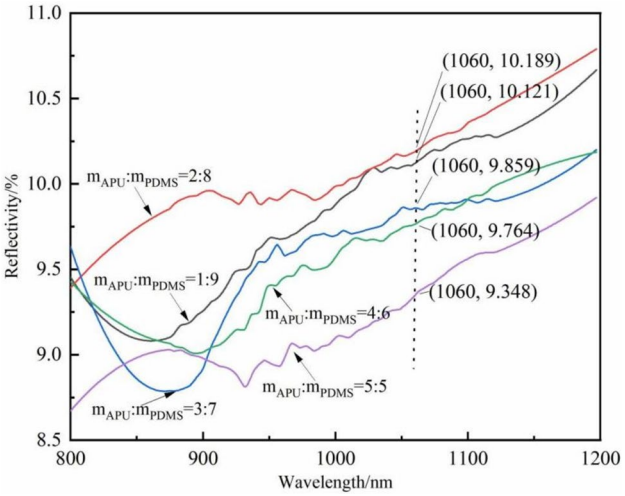

Fig. 14. Near-infrared reflectance spectra of coatings with varying m_{APU}:m_{PDMS} ratios.

m_{APU}:m_{PDMS}	1:9	2:8	3:7	4:6	5:5
Adhesion strength/grade	5	3	2	2	1
Flexibility/mm	3	3	4	6	6
Impact strength/kg × cm	50	50	50	50	50

Table 4. Mechanical properties of coatings with varying m_{APU}:m_{PDMS} ratios.

Effect of DOP on coating properties

Figure 15 shows SEM images of the coatings prepared with DOP additions of 0 wt%, 1 wt%, and 3 wt% under the conditions of m_{APU}:m_{PDMS} of 3:7, m_{Gr}:$M_{nano\text{-}SiO2}$ of 6:4, the total filler addition amount of 40 wt%, and the KH560 addition amount of 4 wt%. It can be seen that the DOP-modified coating has little effect on the surface micro-structure of the coating. Without or with a small amount of DOP, the graphene in the coating is uniformly dispersed, and the nano-SiO_2 is widely distributed, neatly arranged and compact. The bonding between the filler and the resin is appropriate, and the resin thickness is consistent. The size and arrangement of rough structural units on the surface of the coating are uniform.

Figure 16 shows the WCAs of the coatings with DOP additions of 0 wt%, 1 wt%, and 3 wt%. It can be seen that DOP has a certain wetting effect on the coating, as the WCA of the coating decreases from 155° when DOP is not added to the coating to 149° when 3 wt% is added. The reason for this change could be that the addition of DOP introduces some polar ester groups, which increases the surface energy of the coating and thus reduces the WCA. However, even with a 1 wt% DOP addition, the coating maintains a good super-hydrophobic property, with a WCA 152°.

Figure 17 shows the near-infrared reflectance spectra of the coatings with varying DOP additions. The addition of DOP has a slightly positive impact on the absorption of the coating at 1.06 μm near-infrared light, but the resulting change in reflectivity is only 1.356%. The unique molecular structure of DOP contains both polar ester groups and non-polar carbon chains, which enables easy insertion into the resin's molecular chain. This weakens inter-molecular forces within the resin, reduces fine gaps in the coating, and improves filler dispersion. These are conducive to enhancing the absorption of graphene to near-infrared light, so as to achieve the effect of reducing the near-infrared reflectivity of the coating.

Table 5 shows the adhesion strength, flexibility, and impact strength of the coatings with different DOP additions. It can be seen that the addition of DOP significantly improved the flexibility of the coating, from the original 4 mm without DOP to 2 mm (optimal flexibility) when the DOP addition is 5 wt%. The addition of KH560 has maintained the impact strength of the coating at its best, DOP has not influenced the adhesion strength of the coating, which remains at grade 2. The primary factor is that the DOP molecular structure consists of polar ester groups and non-polar carbon chains, facilitating their insertion into the resin molecular chains. This action reduces the inter-molecular force of the resin, the degree of cross-linking between the resin chains after curing, and the brittleness of the coating, thereby greatly enhancing the flexibility of the coating. Based on the above consideration, it is determined that the DOP addition amount is 1 wt%. The optimal DOP addition

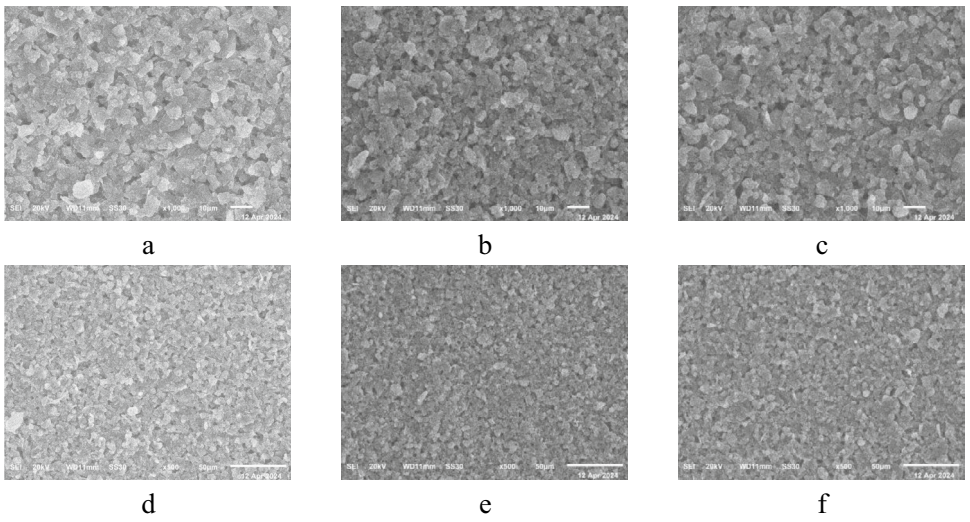

Fig. 15. SEM images of coatings with varying DOP additions, (**a**, **d**) 0 wt%, (**b**, **e**) 1 wt%, and (**c**, **f**) 3 wt%

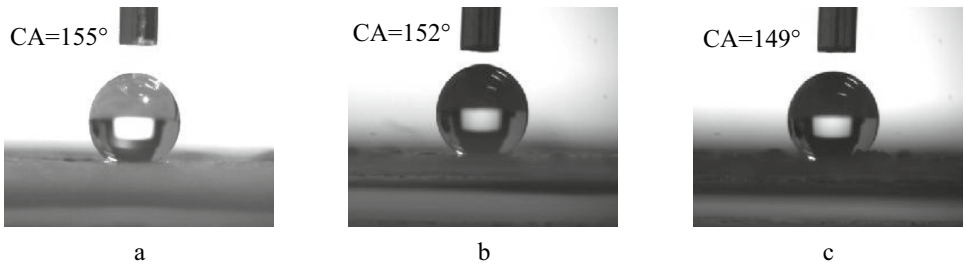

Fig. 16. WCAs of coatings with varying DOP additions, (**a**) 0 wt%, (**b**) 1 wt%, and (**c**) 3 wt%

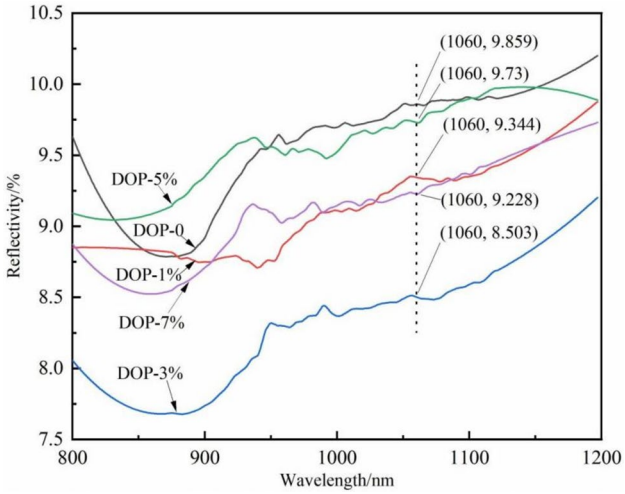

Fig. 17. Near-infrared reflectance spectra of coatings with varying DOP additions.

Contents of DOP/wt%	0	1	3	5	7
Adhesion strength/grade	2	2	2	2	2
Flexibility/mm	4	3	3	2	2
Impact strength/kg × cm	50	50	50	50	50

Table 5. Mechanical properties of coatings with varying DOP additions.

results in a coating with 9.3% near-infrared reflectivity, 152° WCA, grade 2 adhesion strength, 3 mm flexibility, and 50 kg × cm impact strength. The coating meets the design requirements of ultra-low near-infrared reflectivity, super-hydrophobicity, and outstanding mechanical properties.

Conclusions

Using PDMS-modified APU as a binder and graphene as a near-infrared absorber, a super-hydrophobic ultra-low near-infrared reflectivity PDMS-modified APU/ graphene composite coating with WCA greater than 150° and near-infrared reflectivity of 1.06 μm less than 10% was obtained through coating formulation design and modification technology. The following results are obtained by studying the composition and comprehensive properties of the coating:

The reflectivity of the coating at 1.06 μm can be varied from 6.4 to 8.4% and the WCA from 138.5° to 149.5° by modifying the mass ratio of graphene to nano-SiO_2.

By adjusting the total filler addition amount, the reflectivity of the coating at 1.06 μm can be modulated between 4.2 and 13.6%, while the WCA can vary from 98.5° to 152.5° based on the graphene to nano-SiO_2 mass ratio of 6:4.

With further use of KH560 modified coating, the WCA and 1.06 μm near-infrared reflectivity showed limited changes, but the impact strength of the coating increased significantly from 15 to 50 kg × cm.

The hydrophobic and mechanical properties of the coating can be significantly improved by adjusting the mass ratio of APU to PDMS, but the effect on the near-infrared reflectivity of the coating is limited.

By introducing DOP into the coating, the flexibility of the coating can be significantly improved while maintaining its ultra-low near-infrared reflectivity and super-hydrophobic properties.

Under the optimal formulation and modified conditions, the coating simultaneously meets the design requirements of 1.06 μm ultra-low near-infrared reflectivity (9.3%), super-hydrophobicity (WCA 152°), and outstanding mechanical properties (adhesion strength grade 2, flexibility 3 mm, impact strength 50 kg × cm). The coating has enormous potential for use in high-performance laser stealth materials.

Data availability

The datasets used and/or analysed during the current study available from the corresponding authors on request.

Received: 26 June 2024; Accepted: 26 August 2024
Published online: 29 August 2024

References

1. Permeh, S., Lau, K. & Duncan, M. Degradation of coatings for steel in environments susceptible to corrosion associated with fouling. *Struct. Infrastruct. E.* **16**, 1186–1200 (2019).

2. Chiu, C. S. *et al.* Environmental effects on TPB wavelength-shifting coatings. *J. Instrum.* **7**, 07007 (2012).
3. Rauner, N. *et al.* A coating that combines lotus-effect and contact-active antimicrobial properties on silicone. *Adv. Funct. Mater.* **28**, 1801248 (2018).
4. Nine, M. J., Tung, T. T., Alotaibi, F., Tran, D. N. H. & Losic, D. Facile adhesion-tuning of superhydrophobic surfaces between "lotus" and "petal" effect and their influence on icing and deicing properties. *ACS Appl. Mater. Interfaces* **9**, 8393–8402 (2017).
5. Rahman, M. K. *et al.* High-efficiency electrospray deposition method for nonconductive substrates: Applications of superhydrophobic coatings. *ACS Appl. Mater. Interfaces* **13**, 18227–18236 (2021).
6. Zhou, Y. *et al.* Robust superhydrophobic surface based on multiple hybrid coatings for application in corrosion protection. *ACS Appl. Mater. Interfaces* **11**, 6512–6526 (2019).
7. Latthe, S. S. *et al.* Self–cleaning superhydrophobic coatings: Potential industrial applications. *Prog. Org. Coat.* **128**, 52–58 (2019).
8. Rasitha, T. P., Krishna, N. G., Anandkumar, B., Vanithakumari, S. C. & Philip, J. A comprehensive review on anticorrosive/antifouling superhydrophobic coatings: Fabrication, assessment, applications, challenges and future perspectives. *Adv. Colloid Interface* **324**, 103090 (2024).
9. Yuan, W. Z. & Zhang, L. Z. Lattice Boltzmann simulation of droplets impacting on superhydrophobic surfaces with randomly distributed rough structures. *Langmuir* **33**, 820–829 (2017).
10. Hoshian, S., Jokinen, V., Somerkivi, V., Lokanathan, A. R. & Franssila, S. Robust superhydrophobic silicon without a low surface-energy hydrophobic coating. *ACS Appl. Mater. Interfaces* **7**, 941–949 (2014).
11. Alexander, S., Eastoe, J., Lord, A. M., Guittard, F. & Barron, A. R. Branched hydrocarbon low surface energy materials for superhydrophobic nanoparticle derived surfaces. *ACS Appl. Mater. Interfaces* **8**, 660–666 (2015).
12. Malekkhouyan, R. *et al.* The influence of size and healing content on the performance of extrinsic self-healing coatings. *J. Appl. Polym. Sci.* **138**, 49964 (2020).
13. Latthe, S. S. *et al.* Recent developments in air-trapped superhydrophobic and liquid-infused slippery surfaces for anti-icing application. *Prog. Org. Coat.* **137**, 105373 (2019).
14. Meng, S. *et al.* Preparation and properties of high abrasion resistant superhydrophobic coating on the PCB. *Colloid Surface A* **689**, 133674 (2024).
15. Zhang, K., Yang, X., Zhu, N., Wang, Z. C. & Yan, H. Environmentally benign paints for superhydrophobic coatings. *Colloid Polym. Sci.* **295**, 709–714 (2017).
16. Anitha, C., Azim, S. S. & Mayavan, S. Salvinia inspired fluroine free superhydrophobic coatings. *Appl. Surf. Sci.* **449**, 250–260 (2018).
17. Shi, S. H. *et al.* 3D-printed carbon-based conformal electromagnetic interference shielding module for integrated electronics. *Nano-Micro Lett.* **16**, 85 (2024).
18. Shi, S. H. *et al.* Lightweight Zn-Philic 3D-Cu scaffold for customizable zinc ion batteries. *Adv. Funct. Mater.* **34**, 2312664 (2024).
19. Han, P., Huang, X. & Zhang, Q. Laser stealth absorbent of samarium oxysulfide prepared by flux method. *Rare Metals* **30**, 616–620 (2011).
20. Chai, X. *et al.* Silver-modified chromium(III) oxide as multi-band compatible stealth materials for visual/infrared stealth and radar wave transmission. *Compos. Sci. Technol.* **216**, 109038 (2021).
21. Zhuang, Y., Zhang, W. & Zhang, Q. Preparation and characterization of high-performance composite coatings compatible with near-infrared low reflectivity and low infrared emissivity. *Coatings* **13**, 13122033 (2023).
22. Zhang, W., Zhuang, Y. & Zhang, Q. Preparation and properties of multi-color coatings with ultra-low near-infrared reflectivity. *Infrared Phys. Technol.* **136**, 105122 (2024).
23. Wu, H., Zhu, L. N., Yue, W., Fu, Z. Q. & Kang, J. J. Wear-resistant and hydrophobic characteristics of PTFE/CF composite coatings. *Prog. Org. Coat.* **128**, 90–98 (2019).
24. Liu, J., Wang, X., Li, H. & Yang, W. Delamination mechanism maps for coatings/substrates system subjected to adhesive contact loads. *Thin Solid Films* **626**, 159–167 (2017).
25. Ba, M., Zhang, Z. & Qi, Y. The dispersion tolerance of micro/nano particle in polydimethylsiloxane and its influence on the properties of fouling release coatings based on polydimethylsiloxane. *Coatings* **7**, 7070107 (2017).
26. Bai, S., Guan, X., Li, H. & Ou, J. Effect of the specific surface area of nano-silica particle on the properties of cement paste. *Powder Technol.* **392**, 680–689 (2021).
27. Su, H. *et al.* Lotus leaf-like Ni-decorated SiC with combined superhydrophobicity and enhanced microwave absorption performance. *Colloid Surface A* **650**, 129602 (2022).
28. Li, W. *et al.* The effects of interfacial water and SiO_2 surface wettability on the adhesion properties of SiO_2 in epoxy nanocomposites. *Appl. Surf. Sci.* **502**, 144151 (2020).
29. Guo, Q. *et al.* Study on the effects of interfacial interaction on the rheological and thermal performance of silica nanoparticles reinforced epoxy nanocomposites. *Compos. Part B-Eng.* **116**, 388–397 (2017).
30. Lin, Y., Liao, Y., Chen, Z. & Connell, J. W. Holey graphene: A unique structural derivative of graphene. *Mater. Res. Lett.* **5**, 209–234 (2017).
31. Yang, G., Li, L., Lee, W. B. & Ng, M. C. Structure of graphene and its disorders: A review. *Sci. Technol. Adv. Mat.* **19**, 613–648 (2018).
32. Ge, Z., Ren, H., Fu, S. & Chen, S. Synergistic effects of zwitterionic segments and a silane coupling agent on zwitterionic shape memory polyurethanes. *RSC Adv.* **7**, 42320–42328 (2017).
33. Zhang, J., Zhang, W., Guan, Q., Li, X. & Lv, D. Preparation and properties of epoxy resin and polyurethane blend resin-based low-infrared-emissivity coatings. *Coatings* **12**, 12111708 (2022).

Acknowledgements

This work was financially supported by the National Natural Science Foundation of China (61705029) and Key Project of Scientific Research Plan of Higher Education in Anhui Province (2022AH051121).

Author contributions

W.G.Z. designed the overall research scheme, analyzed the obtained data and revised the manuscript. Y.T.Z. prepared the coating samples, tested the near-infrared spectroscopy and wroted the manuscript. J.L.Z. tested the water contact angle and mechanical properties. Q.F.Z. designed the experimental scheme and characterized the micro-structure.

Competing interests

The authors declare no competing interests.

Additional information

Correspondence and requests for materials should be addressed to W.Z.